Semiclassical initial-value-representation study of helium scattering from Cu(110)

Jeremy M. Moix and Eli Pollak*
Department of Chemical Physics, Weizmann Institute of Science, Rehovot 76100, Israel
(Received 26 March 2009; published 16 June 2009)

The final momentum distribution for the scattering of He from a corrugated surface representation of Cu(110) is obtained from semiclassical theory. We derive a formally exact expression for the distribution which involves the absolute value squared of a single overlap of the initial wave function with the final momentum state. This reduces the number of phase-space integrals appearing in the semiclassical expressions and therefore leads to a large reduction in the computational effort. In addition, other energy-dependent observables are directly accessible from the momentum distribution without the need for further simulations. Using this formalism, we compare the quality of results obtained using a classical Wigner approximation and the frozen Gaussian, Herman-Kluk, and thawed Gaussian semiclassical propagators. We find that the thawed Gaussian is not only the best approximation, but it also converges more rapidly than the other semiclassical methods. The frozen Gaussian Herman-Kluk propagator is superior to the frozen Gaussian propagator. In contrast, the classical Wigner approach is qualitatively wrong as it does not properly account for the interference which dominates the angular distribution.

DOI: 10.1103/PhysRevA.79.062507 PACS number(s): 31.15.xg, 34.50.−s

I. INTRODUCTION

The scattering of helium atoms from metal surfaces [1–3] at low energy has been extensively applied as a tool to extract detailed information on surface morphology, adsorbate dynamics, and energy relaxation processes [4–8]. The incoming helium atom interacts weakly with the topmost layers of the surface, and therefore serves as a nondestructive probe that only slightly perturbs the underlying substrate [9]. A measurement of the properties of the scattered beam can yield a wealth of information on the equilibrium structure and dynamics of the surface of the crystal. Surface scattering experiments have been used, for example, as an effective method to determine the form of the many-body atom-surface potential [10,11]. However, the experimental procedures and interpretation of the resulting spectra are nontrivial tasks. Likewise, the theoretical description of the scattering process is challenging [8,12–15]. While the scattering of heavier neon and especially argon atoms behaves mostly classically [16,17], the relatively small mass of helium leads to pronounced quantum-mechanical interference effects.

To simulate the experimental data, ideally one would use an *ab initio* chemistry approach to compute the force field, coupled with an exact quantum dynamics method. Such an ambitious program is still not feasible even with present day computational resources. For numerically exact quantum dynamics one needs the global potential-energy surface. Furthermore, even with multiconfiguration time-dependent Hartree methods [18], the numerical effort grows exponentially with the number of degrees of freedom. An attractive route for overcoming these formidable problems is to use the semiclassical initial value representation (SCIVR) approximation for the dynamics [19–23].

The SCIVR approach has the advantage that the computation may be performed using Monte Carlo methods so that the numerical effort does not scale exponentially with the number of degrees of freedom. Not less important is that the fundamental building blocks of the theory are classical trajectories for which one needs only local force field information. As a result, one may adopt highly attractive "on the fly" methods for the quantum dynamics [24,25]. The main drawback of the SCIVR approach is that it is approximate. Although in principle the SCIVR series representation can be used to obtain the exact quantum dynamics [26], the numerical effort is manageable only if the series converges very rapidly. In the present case of He atom scattering, one must use a quantum approach which correctly accounts for interference. Therefore, the SCIVR approximation route provides a reasonable compromise. A central motivation for this work is to prepare the way for large scale SCIVR computations of He scattering from surfaces.

Quantum mechanics based methods used to describe scattering processes have been reviewed recently in Refs. [12,13]. The exact path-integral expression for the quantum propagator requires a search for all possible paths that connect the initial and final states in a given time. However the contribution to the transition probability from most of these paths is highly oscillatory and as a result their individual impact largely averages out. The semiclassical approximation seeks to find only the paths that provide a meaningful contribution to the integral. Formally this is obtained by a stationary phase analysis of the path-integral expression, and leads to a search for the classical trajectories that connect the initial and final states [21]. This is a great simplification, but several difficulties still remain. Boundary value problems are notoriously difficult to manage from a computational perspective, and become even more so as the size of the system increases.

Miller noted that the difficult boundary-value problem can be substituted for a more amenable phase-space integration over initial conditions [27]. Heller introduced a very simple but surprisingly accurate SCIVR known as the frozen Gaussian approximation that is based on coherent states of a fixed width [28]. However the frozen Gaussian propagator suffers

*eli.pollak@weizmann.ac.il

 ©2009 The American Physical Society

from a rapid loss of normalization. Herman and Kluk deduced that what was missing from Heller's frozen Gaussian approximation was a prefactor containing the elements of the stability matrix [29]. The Herman-Kluk propagator was shown to approximately conserve normalization for relatively long times and has since been applied and tested extensively [23,30–32]. Another class of semiclassical propagators originally suggested by Heller which is also based on coherent states is referred to as thawed Gaussian propagators [21,33,34]. The width parameter in the thawed Gaussian approximation is time dependent and also contains the elements of the monodromy matrix. In contrast to the Herman-Kluk SCIVR the thawed Gaussian SCIVR loses normalization rather rapidly [35]. Both approximations are expensive due to the need of computing the monodromy matrix. For a system with N degrees of freedom, this adds an additional $4N^2$ coupled equations of motion as well as the need to compute the determinant at each step of the computation.

Perhaps one of the most severe criticisms of SCIVR methods until recently was that all of the various approximations lacked a systematic method for improvement. Pollak and co-workers have recently formulated a series representation of the exact quantum propagator where the respective SCIVR is simply the leading-order term [26,36]. This formalism allows one to assess the quality of a particular semiclassical approximation by the rate at which its series converges. The series representation has been successfully applied to several physical systems including the quartic double well, diffraction in a model of the double slit experiment, deep tunneling, the spin boson problem, and vibrational relaxation in dissipative oscillators [36–40]. While the computations are not trivial and can become quite costly, in all these cases the series has been shown to converge rapidly, typically within the first two terms. It is worthwhile to note here that subsequently, Kay derived an asymptotic $\hbar$ dependent series representation of the propagator and has analyzed its performance for several model systems [41–43].

In this work, the low energy scattering of helium atoms from the copper (110) surface is modeled using several semiclassical approximations and a classical Wigner approach. The experimental scattering angle distributions display several peaks of varying intensity depending on the incident angle [9,11,44]. While it is often the case that the Herman-Kluk propagator is the most accurate of the SCIVRs [30,35], here we find that the thawed Gaussian propagator is substantially superior. It agrees almost quantitatively with exact quantum computations. Not less important is the fact that the thawed Gaussian simulations converge with at least 2 orders of magnitude fewer trajectories. While the thawed Gaussian and Herman-Kluk frozen Gaussian approaches are capable of semiquantitatively reproducing the scattering angle distributions at all angles of incidence, the frozen Gaussian SCIVR is much less accurate and the classical Wigner simulations produce qualitatively incorrect results. The latter predicts only two peaks at the rainbow angles while the specular peak, which is often the most intense peak in the angular distribution, is completely absent. The structure seen in the angular distributions is a result of quantum-mechanical interference which has been shown to be rather well described by semiclassical methods [37,45].

In the following section, a formally exact expression for the calculation of the final momentum distribution and subsequently, the angular distribution, is presented. It casts the semiclassical expression in a particularly simple form which leads to a reduction in the number of phase-space integrations required to calculate the momentum distribution. This removes some of the serious difficulties encountered with previous approaches. The direct computation of the final momentum distribution has the advantage that other energy-dependent quantities are also immediately available without the need to carry out any further simulations. The various semiclassical propagators used in the scattering angle distribution calculations are also introduced in this section. Numerical results of the semiclassical and classical simulations are presented in Sec. III. We end with a discussion of the merits and possible further applications of the SCIVR approach to surface scattering.

II. SCATTERING FORMALISM

A. Scattering angle distribution

We will restrict ourselves to a two-dimensional model of the system involving the scattering coordinate perpendicular to the surface and a transverse coordinate parallel to the surface. This model is appropriate for in-plane scattering experiments at low surface temperatures, such that at zeroth order the interaction with surface phonons can be ignored. The traditional approach to calculating the angular scattering distribution is written in terms of the correlation function [45]

$$P(\theta) = \lim_{t\to\infty} \mathrm{Tr}[|\psi\rangle\langle\psi|\hat{K}^{\dagger}(t)\delta(\theta-\hat{\theta})K(t)], \tag{1}$$

where the angle operator $\hat{\theta}=\tan^{-1}(\frac{\hat{p}_x}{\hat{p}_z})$, ψ characterizes the initial wave packet of the scattering atom and $K(t)$ is the quantum propagator. However, the angle operator can prove to be troublesome from a computational perspective when implemented in semiclassical approximations.

As an alternative, the angular distribution can be written in terms of an intermediate two-dimensional distribution in polar coordinates as

$$P(\theta) = \int_0^{\infty} P(p,\theta)pdp. \tag{2}$$

In the natural Cartesian coordinates of the simulation, $P(p,\theta)$ carries over to the final Cartesian momentum distribution $P(p_x,p_z)$ with $p_x=p\sin(\theta)$ and $p_z=p\cos(\theta)$. Then the central quantity to calculate becomes

$$\begin{aligned} P(\bar{p}_x,\bar{p}_z;t) &= \mathrm{Tr}[|\psi\rangle\langle\psi|\hat{K}^{\dagger}(t)\delta(\bar{p}_x-\hat{p}_x)\delta(\bar{p}_z-\hat{p}_z)K(t)] \\ &= |\langle\bar{p}_x,\bar{p}_z|K(t)|\psi\rangle|^2 \equiv |I(\bar{p}_x,\bar{p}_z;t)|^2, \end{aligned} \tag{3}$$

and this defines the overlap function $I(\bar{p}_x,\bar{p}_z;t)$. The momentum operators commute so there is no ambiguity in this definition. Introducing the final momentum distribution reduces the numerical effort to the evaluation of a single overlap function that contains only one time propagation. As a result, only a single phase-space integration is required in the SCIVR approximation leading to a large reduction in the computational effort. The final angular distribution is then obtained from Eq. (2) after an additional numerical integration over the radial momentum. The momentum distribution is well-behaved numerically and has the additional advantage that other energy-dependent quantities such as the energy-loss distribution are immediately available from $P(\bar{p}_x,\bar{p}_z)$ without the need for any further semiclassical calculations. For in-plane scattering, introducing the requisite two-dimensional fixed grid of momentum points is not an issue.

B. Semiclassical initial value representations

The frozen Gaussian, Herman-Kluk, and thawed Gaussian SCIVR propagators can all be written in the generic form,

$$\hat{K}_0(t)|g(\mathbf{p},\mathbf{q};0)\rangle = R(\mathbf{p},\mathbf{q};t)e^{(i/\hbar)W(\mathbf{p},\mathbf{q};t)}|g(\mathbf{p},\mathbf{q};t)\rangle, \quad (4)$$

where the coordinate representation of the coherent states is

$$\langle \mathbf{x}|g(\mathbf{p},\mathbf{q})\rangle = \left(\frac{\det \mathrm{Re}\,\boldsymbol{\Gamma}(t)}{\pi^N}\right)^{1/4} \exp\left(-\frac{1}{2}(\mathbf{x}-\mathbf{q})^{\mathrm{T}}\boldsymbol{\Gamma}(t)(\mathbf{x}-\mathbf{q}) + \frac{i}{\hbar}\mathbf{p}^{\mathrm{T}}(\mathbf{x}-\mathbf{q})\right), \quad (5)$$

and N is the total number of degrees of freedom in the system. For future use, we also note the momentum representation of the coherent states,

$$\langle \bar{\mathbf{p}}|g(\mathbf{p},\mathbf{q})\rangle = \left(\frac{1}{\pi\hbar^2}\right)^{N/4}\left(\frac{\det \mathrm{Re}\,\boldsymbol{\Gamma}(t)}{\det|\boldsymbol{\Gamma}(t)|^2}\right)^{1/4} \times \exp\left(-\frac{1}{2\hbar^2}(\bar{\mathbf{p}}-\mathbf{p})^{\mathrm{T}}\boldsymbol{\Gamma}(t)^{-1}(\bar{\mathbf{p}}-\mathbf{p}) - \frac{i}{\hbar}\mathbf{q}^{\mathrm{T}}\bar{\mathbf{p}}\right). \quad (6)$$

The differences between the propagators which will be specified below are borne out in the Hamiltonian governing the classical dynamics and the definitions of the prefactor R, the action W, and the width matrix $\boldsymbol{\Gamma}$.

Introducing the notation $\mathbf{Y}=(\mathbf{p},\mathbf{q})$ and $d\mathbf{Y}=d\mathbf{p}d\mathbf{q}/(2\pi\hbar)^N$, the zeroth order semiclassical expression for the momentum overlap function in terms of the generic propagator Eq. (4) can be written as

$$I_0(\bar{p}_x,\bar{p}_z;t) = \frac{1}{\sqrt{N(t)}}\int_{-\infty}^{\infty} d\mathbf{Y}\langle \bar{p}_x,\bar{p}_z|g(\mathbf{Y};t)\rangle \times \langle g(\mathbf{Y})|\psi\rangle R(\mathbf{Y};t)\exp\left(\frac{i}{\hbar}W(\mathbf{Y};t)\right). \quad (7)$$

The SCIVR propagators studied here are not unitary so one must renormalize with the function $N(t)$ defined as

$$N(t) = \mathrm{Tr}\langle\psi|K_0^{\dagger}(t)K_0(t)|\psi\rangle. \quad (8)$$

Alternatively, the normalization function may be obtained more efficiently by simply integrating the momentum distribution at each step during the calculation. For the zeroth order SCIVR, it is sufficient to renormalize only the final momentum distribution so that the added effort of renormalization is negligible.

1. Prefactor-free frozen Gaussian propagator

The simplest SCIVR approximation is the frozen Gaussian propagator [28]. As the name implies, the prefactor $R_{\mathrm{FG}}(\mathbf{p},\mathbf{q};t)=1$, and the width matrix in the coherent states is time independent so that the widths of the Gaussians are "frozen" throughout the propagation. To ensure integrability, $\boldsymbol{\Gamma}_{\mathrm{FG}}$ must be positive definite. We will assume that it is diagonal with positive elements. The action term appearing in the frozen Gaussian propagator involves the coherent-state averaged Hamiltonian

$$W_{\mathrm{FG}}(\mathbf{p},\mathbf{q};t) = \int_0^t dt'[\mathbf{p}(t')\dot{\mathbf{q}}(t') - \langle g(\mathbf{p},\mathbf{q};t')|\hat{H}|g(\mathbf{p},\mathbf{q};t')\rangle]. \quad (9)$$

The dynamics is governed by the Wigner representation of the Hamiltonian operator.

2. Herman-Kluk frozen Gaussian propagator

Although very simple to implement, the prefactor-free propagator suffers from a rapid loss of normalization. In an attempt to address this deficiency, the Herman-Kluk SCIVR includes a prefactor containing the elements of the stability matrix [29],

$$R_{\mathrm{HK}}(\mathbf{p},\mathbf{q};t) = \sqrt{2^{-N}\det\left[\left(\frac{\partial\mathbf{q}(t)}{\partial\mathbf{q}(0)}\right) + \boldsymbol{\Gamma}^{-1}\left(\frac{\partial\mathbf{p}(t)}{\partial\mathbf{p}(0)}\right)\boldsymbol{\Gamma} + \frac{i}{\hbar}\boldsymbol{\Gamma}^{-1}\left(\frac{\partial\mathbf{p}(t)}{\partial\mathbf{q}(0)}\right) - i\hbar\left(\frac{\partial\mathbf{q}(t)}{\partial\mathbf{p}(0)}\right)\boldsymbol{\Gamma}\right]}. \quad (10)$$

In general, including the prefactor leads to simulations that are approximately unitary for relatively long times. The action in the Herman-Kluk propagator takes the standard form,

$$W_{\mathrm{HK}}(\mathbf{p},\mathbf{q};t)=\int_0^t dt'[\mathbf{p}(t')\dot{\mathbf{q}}(t')-H]. \tag{11}$$

As with the frozen Gaussian propagator, the width matrix in the coherent states is taken to be constant and diagonal with positive elements. The dynamics takes place on the Wigner representation of the Hamiltonian operator, although in principle, one may also define a Herman-Kluk like SCIVR in which the dynamics is governed by the coherent-state representation of the Hamiltonian operator [46].

3. Thawed Gaussian propagator

The thawed Gaussian propagator is distinguished from the previous two frozen Gaussian propagators in that the width matrix is allowed to be time dependent. In this case, $\mathbf{\Gamma}_{\mathrm{TG}}(t)$ is restricted to be symmetric and positive definite although it is generally complex valued. Following Gelabert *et al.* the width matrix can be written in terms of the elements of the monodromy matrices by defining two auxiliary terms [47],

$$\mathbf{Q}(t)=\left(\frac{\partial\mathbf{q}(t)}{\partial\mathbf{q}(0)}\right)+i\hbar\left(\frac{\partial\mathbf{q}(t)}{\partial\mathbf{p}(0)}\right)\mathbf{\Gamma}_{\mathrm{TG}}(0),$$

$$M\dot{\mathbf{Q}}(t)=\left(\frac{\partial\mathbf{p}(t)}{\partial\mathbf{q}(0)}\right)+i\hbar\left(\frac{\partial\mathbf{p}(t)}{\partial\mathbf{p}(0)}\right)\mathbf{\Gamma}_{\mathrm{TG}}(0), \tag{12}$$

where M is the mass. The width matrix may now be written compactly as

$$\frac{i\hbar}{M}\mathbf{\Gamma}_{\mathrm{TG}}(t)=\dot{\mathbf{Q}}(t)\mathbf{Q}(t)^{-1}, \tag{13}$$

and similarly, the prefactor can be represented simply as

$$R_{\mathrm{TG}}(\mathbf{p},\mathbf{q};t)=\left(\frac{\det \mathrm{Re}[\mathbf{\Gamma}_{\mathrm{TG}}(0)]}{\det \mathrm{Re}[\mathbf{\Gamma}_{\mathrm{TG}}(t)]}\right)^{1/4}\frac{1}{\sqrt{\det \mathbf{Q}(t)}}. \tag{14}$$

One then distinguishes between two different thawed Gaussian approximations. The Wigner thawed Gaussian (WTG) approximation has a classical dynamics which is evolved from the Wigner representation of the Hamiltonian operator. In this case the action term is the same as in the Herman-Kluk propagator. The other approximation is the coherent-state thawed Gaussian approximation suggested by Baranger *et al.* [21] and generalized to multidimensional systems in Ref. [34], in which the classical dynamics is derived from the coherent-state representation of the Hamiltonian operator. The action term then includes the time integral over the coherent state averaged quantities. In Ref. [26], the coherent-state thawed Gaussian was shown to be more accurate than the Wigner thawed Gaussian or Herman-Kluk propagator at short times.

C. Classical Wigner approximation

In the classical Wigner (or linearized SCIVR) approximation [48–50], the initial conditions for the system are treated quantum mechanically, but the ensuing time evolution is replaced by classical dynamics. The Wigner representation for the momentum distribution

$$P_{\mathrm{W}}(\bar{p}_x,\bar{p}_z;t)=2\pi\hbar\int_{-\infty}^{\infty}d\mathbf{p}d\mathbf{q}\Psi(\mathbf{p},\mathbf{q})\delta(\bar{p}_x-p_x(t))\times\delta(\bar{p}_z-p_z(t)), \tag{15}$$

requires only a single phase-space integration for the system variables. The initial state of the system $\Psi(\mathbf{p},\mathbf{q})$ is given by the Wigner transform of the initial wave packet,

$$\Psi(\mathbf{p},\mathbf{q})=\frac{1}{(2\pi\hbar)^N}\int_{-\infty}^{\infty}d\boldsymbol{\xi}e^{(i/\hbar)\mathbf{p}^{\mathrm{T}}\boldsymbol{\xi}}\left\langle\mathbf{q}+\frac{\boldsymbol{\xi}}{2}|\psi\right\rangle\left\langle\psi|\mathbf{q}-\frac{\boldsymbol{\xi}}{2}\right\rangle. \tag{16}$$

As there are no phases appearing in the classical Wigner calculations, the calculations typically converge much more rapidly than the semiclassical simulations.

III. SCATTERING CALCULATIONS

A. Scattering model

The Hamiltonian for the scattering system has the standard form

$$H=\frac{p_x^2+p_z^2}{2M}+V(x,z), \tag{17}$$

where M is the mass of the helium atom. The model potential is taken as the modified corrugated Morse potential (MCMP) developed by Salanon *et al.* [11]

$$V(x,z)=V_0(e^{-2\alpha z}-2e^{-\alpha z}+1)+V_0V_{\mathrm{c}}e^{-3\alpha z}\cos(2\pi x/l). \tag{18}$$

The well depth of the Morse potential is $V_0=6.35$ meV and the inverse length is $\alpha=1.05$ Å^{-1}, such that the isolated system would support two bound states. The Cu(110) lattice length is $l=3.6$ Å and the dimensionless corrugation coefficient is $V_{\mathrm{c}}=0.0255$. The initial wave packet of the incoming helium atom is chosen to be a Gaussian coherent state whose coordinate representation is

$$\langle x,z|\psi\rangle=\left(\frac{\gamma_x\gamma_z}{\pi^2}\right)^{1/4}e^{-(\gamma_x/2)(x-x_0)^2-(\gamma_z/2)(z-z_0)^2+(i/\hbar)p_{x_0}(x-x_0)+(i/\hbar)p_{z_0}(z-z_0)}. \tag{19}$$

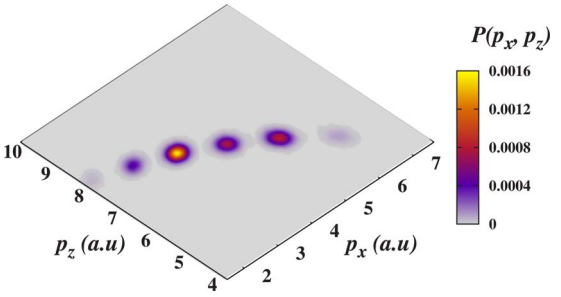

FIG. 1. (Color online) The zeroth order semiclassical momentum distribution calculated at an incident scattering angle of 32.5° using the Wigner thawed Gaussian propagator.

The center of the wave packet (x_0, z_0) is chosen to be sufficiently far from the surface that $V(x,z)$ is negligible for all trajectories. The initial momenta of the wave packet are defined by the initial energy of the beam (125 meV) and the specified scattering angle. The width parameters for the initial wave packet are taken to be $\gamma_x = \gamma_z \equiv \gamma = 0.05$ a.u.$^{-2}$ and the width parameters for the coherent states are $\Gamma_x = \Gamma_z = 10\gamma$ in all of the computations presented below. The specific choice for these parameters is a tradeoff between the need to define the momenta of the original wave packet rather narrowly, while at the same time the coherent states should be defined on a length scale which does not smear out the corrugation potential.

Outside the interaction regime, the free particle motion of the trajectories is integrated analytically for efficiency. At the lowest scattering angle studied of 32.5° (defined relative to the surface normal), a simulation time of 10 ps was needed in order to ensure that all particles had escaped from the interaction regime. At a larger incident angle of 50.5°, 20 ps simulations were required and this lengthened to 40 ps at a scattering angle of 65.5°. The simulation length is not an issue in this case since only the final phase-space points of the trajectories are required and a large part of the propagation can be performed analytically. The spatial width of the wave packet was sufficiently larger than the lattice length so there was no further need to average over the impact parameter (horizontal center of the Gaussian wave packet).

B. Numerical results

The final momentum distribution calculated from the Wigner thawed Gaussian approximation at an incidence angle of 32.5° is presented in Fig. 1. The scattering angle distribution obtained after the subsequent integration over the radial momenta is displayed in the lower portion of Fig. 2, along with the results of the coherent-state thawed Gaussian (CSTG) SCIVR approximation and the exact quantum-mechanical values reported in Ref. [11]. As can be seen, the regions of large intensity in the momentum distribution are directly related to the distinct peaks in the angular distribution. The frozen Gaussian (FG), Herman-Kluk Frozen Gaussian (HKFG), and the classical Wigner approximations are compared with the exact results in the top panel of Fig. 2.

As noted many times before, both the frozen and thawed Gaussian propagators suffer from a rapid loss of normalization, but nevertheless, all of the semiclassical scattering angle distributions need to be renormalized. The Herman-Kluk propagator required 10^7 trajectories to achieve a variance of 1% in the momentum distribution calculations, the frozen Gaussian results required 10^6, while each of the thawed Gaussian approximations and the classical Wigner dynamics needed only 10^5 trajectories to reach a similar level of convergence. As a result, the thawed Gaussian simulations are the most computationally efficient of the semiclassical methods even with the need to calculate the additional time dependent width matrix.

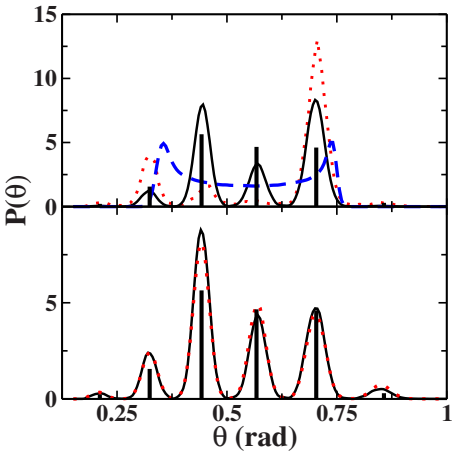

FIG. 2. (Color online) The scattering angle distributions calculated at an incident scattering angle of 32.5°. The exact quantum-mechanical results adapted from Ref. [11] are depicted as sticks. The top panel displays the results of the Herman-Kluk frozen Gaussian propagator as solid lines, the frozen Gaussian as the (red) dotted line, and classical Wigner results as the (blue) dashed line. The bottom panel displays the results of the Wigner thawed Gaussian as solid lines and the coherent-state thawed Gaussian as (red) dotted lines.

As can be seen in Fig. 2, the frozen Gaussian propagator yields results of rather poor quality compared with the other semiclassical approximations. Much of the structure seen in the exact scattering angle distribution is either missing or of incorrect intensity in this case. The results of the thawed Gaussian propagators on the other hand are significantly superior to those of the HKFG. As shown below, similar behavior for the frozen and thawed Gaussian propagators is observed at other scattering angles as well. As mentioned in Sec. II B, the CSTG SCIVR has been shown to be more accurate than the WTG at short times [26]. The same is also true here for the full scattering computation, although the improvement over the WTG results is not very substantial. As noted below, since the WTG does not require any coherent-state averaging it is easier to implement for on the fly computations.

There is a subtle but significant difference between the frozen Gaussian and the thawed Gaussian propagators. Both are exact in the region where the atom is free of the interaction with the surface. However, the Herman Kluk approximation becomes exact only after integration over the phase space, while the thawed Gaussian is already exact for each individual coherent state. In terms of the "correction opera-

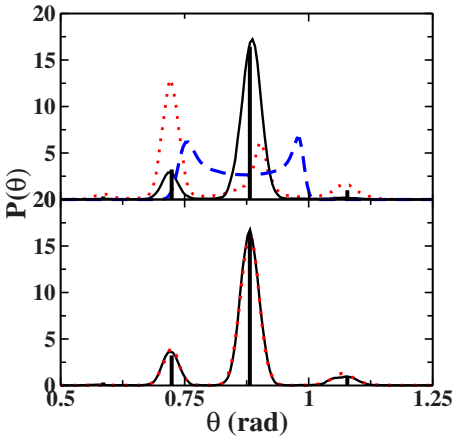

FIG. 3. (Color online) Scattering angle distributions at an incident angle of 50.5°. The other notation is the same as in Fig. 2.

tor" used to construct the series representation of the SCIVR, one finds for a free particle that the potential difference operator vanishes at each point in-phase space for the thawed Gaussian, while for the HKFG it vanishes only after integration over the whole phase space. As a result substantially more averaging is needed in order to obtain the same level of accuracy for the latter. The conclusion is that while considering bound-state systems, one should perhaps use the Herman-Kluk SCIVR, whereas in scattering problems, the thawed Gaussian form is superior.

The angular distributions obtained at the incidence angles of 50.5° and 65.5° are presented in Figs. 3 and 4, respectively. Although not shown, their corresponding momentum distributions display the expected behavior. Here too, we included the results of the classical Wigner calculations from Eq. (15) and the exact quantum-mechanical values as given in Ref. [11]. The number of Monte Carlo samples need to obtain convergence for each propagator at the higher incidence angles is the same as those mentioned above for the case of 32.5°, except a five- and tenfold increase was needed for the FG approximation at 50.5° and 65.5°, respectively. At these higher incidence angles, the peak locations calculated from both of the frozen Gaussian propagators begin to display a small shift toward higher scattering angles when compared with the exact results. This is particularly evident for the FG approximation at 65.5°, although it is also observed at the lower scattering angles and for the HKFG results as well. Both of the thawed Gaussian SCIVRs still reproduce the correct location again indicating their superior performance over the frozen Gaussian propagators for helium scattering.

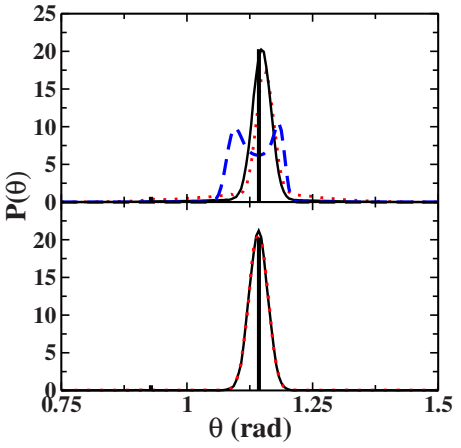

FIG. 4. (Color online) Scattering angle distributions at an incident angle of 65.5°. The other notation is the same as in Fig. 2.

IV. DISCUSSION

This work is another demonstration of the ability of the semiclassical initial value representation to describe quantum interference effects. In previous work it was shown that the SCIVR methodology accounts well for interference in a model of the double slit experiment [45]. At all three incidence angles presented, the semiclassical simulations faithfully reproduce the qualitative features of the exact quantum-mechanical results. The SCIVR calculations yield the same number and location of peaks as the exact results, but the intensities are in good agreement only when using the thawed Gaussian approximations. These results indicate that the semiclassical description provides a reliable estimate to the exact angle distributions. Although not reported, similar behavior of the semiclassical and classical models has been observed at other energies and for a slightly different form of the potential as well.

Four different semiclassical propagators and a classical Wigner approximation were used to calculate the scattering angle distribution. Although in many situations the Herman-Kluk propagator is seen to be the most accurate SCIVR, here we found that the thawed Gaussian approximations produce more accurate results and converge much more quickly. The particular choice of coherent-state width parameter does not strongly influence the accuracy of the HKFG. Only small changes in the peak heights were observed for variations of Γ over 2 orders of magnitude. The frozen Gaussian approximation does account for interference effects but it is inferior when compared to the other semiclassical methods. Although cheaper, the classical Wigner simulations are completely inadequate and produce qualitatively incorrect angle distributions. At all incidence angles studied, the Wigner calculations display a minimum at the specular angle, although this is often the most intense peak in the spectrum. The structure seen in the angle distributions arises from quantum-mechanical interferences which the classical Wigner model is not able to reproduce.

Introducing the intermediate momentum distribution results in several computational and analytical simplifications. Taking this approach instead of directly calculating the angle distribution allows one to calculate other energy-dependent quantities without the need for any additional semiclassical simulations. From a computational perspective, the reduced number of phase-space integrations that result at each order in an SCIVR series representation of the exact propagator leads to much more amenable simulations.

In this work, the surface phonons were ignored. It is in principle straightforward to include a harmonic phonon bath in the SCIVR framework. However, the resulting semiclas-

sical expression is no longer as simple. To obtain the final system momentum distribution in the presence of a bath, one introduces a generalized distribution as before

$$P(\bar{p}_x,\bar{p}_z;t)=\int_{-\infty}^{\infty} d\bar{\mathbf{p}}_{\mathrm{B}} P(\bar{p}_x,\bar{p}_z,\bar{\mathbf{p}}_{\mathrm{B}};t). \tag{20}$$

An integration over any other suitable bath variables can be used instead of the momenta. For this example the semiclassical momentum distribution becomes

$$P(\bar{p}_x,\bar{p}_z;t)=\int_{-\infty}^{\infty} d\bar{\mathbf{p}}_{\mathrm{B}}\ \mathrm{Tr}\left(\frac{e^{-\beta\hat{H}_{\mathrm{B}}}}{Z_{\mathrm{B}}}|\psi\rangle\langle\psi|\hat{K}_0^{\dagger}(t)\right.$$
$$\left.\times\delta(\bar{p}_x-\hat{p}_x)\delta(\bar{p}_z-\hat{p}_z)\delta(\bar{\mathbf{p}}_{\mathrm{B}}-\hat{\mathbf{p}}_{\mathrm{B}})K_0(t)\right) \tag{21}$$

$$=\int_{-\infty}^{\infty} d\bar{\mathbf{p}}_{\mathrm{B}} d\mathbf{Y}_{\mathrm{B}} \prod_{j=1}^{N_{\mathrm{B}}} \alpha_j \exp\left(-\frac{\alpha_j}{2\hbar\omega_j}(p_j^2+\omega_j^2 x_j^2)\right)$$
$$\times\left|\int_{-\infty}^{\infty} d\mathbf{Y}_{\mathrm{S}}\langle\bar{p}_x,\bar{p}_z,\bar{\mathbf{p}}_{\mathrm{B}}|g(\mathbf{Y};t)\rangle\right.$$
$$\left.\times\langle g(\mathbf{Y}_{\mathrm{S}})|\psi\rangle R(\mathbf{Y};t)\exp\left(\frac{i}{\hbar}W(\mathbf{Y};t)\right)\right|^2, \tag{22}$$

where the coherent-state representation of the Boltzmann operator has been used and $\alpha_j=e^{\hbar\beta\omega_j}-1$ [51]. In the case of scattering, the assumption of factorized initial conditions used here is exact since the helium atom and the surface are initially uncoupled. Equation (22) has the advantage that when integrating over the bath variables, one has a positive integrand. On the other hand, in this approach one must compute the overlap function for each choice of the initial bath variables and this may become costly. As we have seen in this paper, converging a single overlap function using the thawed Gaussian typically requires 10^4–10^5 Monte Carlo trajectories. Averaging over the bath would presumably take an additional 100–1000 samples.

Alternatively one could use the forward-backward formalism in its discretized [52] or continuum form [53]. In the former one has only a single phase-space integration over the bath variables and there is no need for the added bath momentum integration. In the latter one has only a phase-space integration over the system and an averaging with respect to the noise realizations. However, the quantum memory functions can be long, making such a computation also rather costly. A comparison of the different methodologies will be reported elsewhere [54].

As mentioned in the Introduction, the computations reported here are a precursor to the computation of He atom scattering from more realistic surfaces using on-the-fly methods. The results here indicate that on the fly computations, at least for frozen surfaces should be feasible when using the Wigner thawed Gaussian propagator. To implement the Wigner thawed Gaussian propagator one does need the Hessian of the potential-energy surface and this is rather expensive. In this context, it is worth mentioning the development of graphics processor units for use in the Monte Carlo computations needed in the SCIVR methodology. Our preliminary computations for the classical Wigner and frozen Gaussian SCIVR using the CUDA software of NVIDIA show that a single (TESLA) GPU can lead to a 30- to 50-fold enhancement in speed. This added speed may overcome the long time needed to compute a single trajectory using on the fly methods.

ACKNOWLEDGMENTS

We thank Professor S. Miret-Artès and Dr. Santanu Sengupta for fruitful discussions. We also thank Professor T. Martinez for pointing out to us the potential advantages of computations with GPU processors. This work was supported by grants from the Israel Science Foundation and the German Israel Foundation for Basic Research.

[1] *Helium Atom Scattering from Surfaces*, edited by E. Hulpke, Springer Series in Surface Sciences Vol. 27 (Springer, Berlin, 1992).
[2] G. Benedek and J. P. Toennies, Surf. Sci. **299–300**, 587 (1994).
[3] B. Gumhalter, Phys. Rep. **351**, 1 (2001).
[4] J. Lapujoulade, Surf. Sci. Rep. **20**, 195 (1994).
[5] D. Farìas and K.-H. Rieder, Rep. Prog. Phys. **61**, 1575 (1998).
[6] A. Jardine, J. Ellis, and W. Allison, J. Phys.: Condens. Matter **14**, 6173 (2002).
[7] A. P. Graham, Surf. Sci. Rep. **49**, 115 (2003).
[8] R. B. Gerber, Chem. Rev. **87**, 29 (1987).
[9] D. Gorse, B. Salanon, F. Fabre, A. Kara, J. Perreau, G. Armand, and J. Lapujoulade, Surf. Sci. **147**, 611 (1984).
[10] J. A. Barker and D. J. Auerbach, Surf. Sci. Rep. **4**, 1 (1984).
[11] B. Salanon, G. Armand, J. Perreau, and J. Lapujoulade, Surf. Sci. **127**, 135 (1983).
[12] R. Guantes, A. S. Sanz, J. Margalef-Roig, and S. Miret-Artès, Surf. Sci. Rep. **53**, 199 (2004).
[13] A. S. Sanz and S. Miret-Artès, Phys. Rep. **451**, 37 (2007).
[14] J. R. Manson, Comput. Phys. Commun. **80**, 145 (1994).
[15] J. R. Manson, in *Handbook of Surface Science*, edited by N. V. Richardson and Stephen Holloway, Surface Dynamics Vol. 3, edited by Eckart Hasselbrink and Bengt Lundqvist (Elsevier, Amsterdam, 2008).
[16] E. Pollak, S. Sengupta, and S. Miret-Artès, J. Chem. Phys. **129**, 054107 (2008).
[17] E. Pollak and S. Miret-Artès J. Chem. Phys. **130**, 194710 (2009).
[18] H.-D. Meyer and G. A. Worth, Theor. Chem. Acc. **109**, 251 (2003).
[19] F. Grossmann, Comments At. Mol. Phys. **34**, 141 (1999).

[20] D. J. Tannor and S. Garaschuk, Annu. Rev. Phys. Chem. **51**, 553 (2000).
[21] M. Baranger, M. A. M. de Aguiar, F. Keck, H. J. Korsch, and B. Schellhaaß, J. Phys. A **34**, 7227 (2001).
[22] W. H. Miller, J. Phys. Chem. A **105**, 2942 (2001).
[23] K. G. Kay, Annu. Rev. Phys. Chem. **56**, 255 (2005).
[24] M. Ceotto, S. Atahan, S. Shim, G. F. Tantardini, and A. Asparu-Guzik, Phys. Chem. Chem. Phys. **11**, 3861 (2009).
[25] J. Tatchen and E. Pollak, J. Chem. Phys. **130**, 041103 (2009).
[26] E. Pollak and J. Shao, J. Phys. Chem. A **107**, 7112 (2003).
[27] W. H. Miller, J. Chem. Phys. **53**, 3578 (1970).
[28] E. J. Heller, J. Chem. Phys. **75**, 2923 (1981).
[29] M. F. Herman and E. Kluk, Chem. Phys. **91**, 27 (1984).
[30] K. G. Kay, J. Chem. Phys. **100**, 4432 (1994).
[31] W. H. Miller, J. Chem. Phys. **125**, 132305 (2006).
[32] M. Thoss and H. Wang, Annu. Rev. Phys. Chem. **55**, 299 (2004).
[33] E. J. Heller, J. Chem. Phys. **62**, 1544 (1975).
[34] E. Pollak and S. Miret-Artés, J. Phys. A **37**, 9669 (2004).
[35] C. Harabati, J. M. Rost, and F. Grossmann, J. Chem. Phys. **120**, 26 (2004).
[36] S. Zhang and E. Pollak, Phys. Rev. Lett. **91**, 190201 (2003).
[37] S. Zhang and E. Pollak, J. Chem. Phys. **121**, 3384 (2004).
[38] D. H. Zhang and E. Pollak, Phys. Rev. Lett. **93**, 140401 (2004).
[39] E. Martin-Fierro and E. Pollak, J. Chem. Phys. **126**, 164108 (2007).
[40] J. M. Moix and E. Pollak, J. Chem. Phys. **129**, 064515 (2008).
[41] K. G. Kay, Chem. Phys. **322**, 3 (2006).
[42] G. Hochman and K. G. Kay, Phys. Rev. A **73**, 064102 (2006).
[43] G. Hochman and K. G. Kay, J. Chem. Phys. **130**, 061104 (2009).
[44] J. Perreau and J. Lapujoulade, Surf. Sci. **122**, 341 (1982).
[45] R. Gelabert, X. Giménez, M. Thoss, H. Wang, and W. H. Miller, J. Chem. Phys. **114**, 2572 (2001).
[46] E. Martin-Fierro and J. M. G. Llorente, Chem. Phys. **322**, 13 (2006).
[47] R. Gelabert, X. Giménez, M. Thoss, H. Wang, and W. H. Miller, J. Phys. Chem. A **104**, 10321 (2000).
[48] V. S. Filinov, Y. V. Medvedev, and V. L. Kamskyi, Mol. Phys. **85**, 711 (1995).
[49] J. Shao, J.-L. Liao, and E. Pollak, J. Chem. Phys. **108**, 9711 (1998).
[50] X. Sun, H. Wang, and W. H. Miller, J. Chem. Phys. **109**, 7064 (1998).
[51] E. Pollak and E. Martin-Fierro, J. Chem. Phys. **126**, 164107 (2007).
[52] E. Martin-Fierro and E. Pollak, J. Chem. Phys. **125**, 164104 (2006).
[53] E. Pollak, J. Chem. Phys. **127**, 074505 (2007).
[54] J. M. Moix and E. Pollak (unpublished).